Positron driven high-field terahertz waves via dielectric wakefield interaction

N. Majernik,[1] G. Andonian,[1] O. B. Williams,[1] B. D. O'Shea,[2] P. D. Hoang,[1] C. Clarke,[2] M. J. Hogan,[2] V. Yakimenko,[2] and J. B. Rosenzweig[1]

[1]*UCLA Department of Physics and Astronomy, Los Angeles, California 90095, USA*

[2]*SLAC National Accelerator Laboratory, Menlo Park, California 94025, USA*

(Received 9 November 2021; accepted 7 April 2022; published 25 April 2022)

Advanced acceleration methods based on wakefields generated by high-energy electron bunches passing through dielectric-based structures have demonstrated $>$ GV/m fields, paving the first steps on a path to applications such as future compact linear colliders. For a collider scenario, it is desirable that, in contrast with plasmas, wakefields in dielectrics do not behave differently for positron and electron bunches. In this article, we present measurements of large amplitude fields excited by positron bunches with collider-relevant parameters (energy 20 GeV and 0.7×10^{10} particles per bunch) in a 0.4 THz, cylindrically symmetric dielectric structure. Interferometric measurements of emitted coherent Cerenkov radiation permit spectral characterization of the positron-generated wakefields, which are compared to those excited by electron bunches. Statistical equivalence tests are incorporated to show the charge-sign invariance of the induced wakefield spectra. Transverse effects on positron beams resulting from off-axis excitation are examined and found to be consistent with the known linear response of the DWA system. The results are supported by numerical simulations and demonstrate high-gradient wakefield excitation in dielectrics for positron beams.

DOI: 10.1103/PhysRevResearch.4.023065

I. INTRODUCTION

Relativistic positrons and electrons in high-luminosity linear colliders are essential tools for fundamental studies in particle and nuclear physics. The large electron positron (LEP) collider at CERN operated at up to 209 GeV center of mass energy [1]; however, yet higher energy enables important studies into high-precision fundamental particle mass measurements, exotic Higgs particle couplings [2], the search for dark matter [3], or physics beyond the standard model [4]. Achieving TeV-scale center-of-mass energy for positron-electron collisions in a practical footprint [5,6] is a major challenge given existing radio-frequency (RF) acceleration technologies, which are limited by material breakdown to accelerating gradients of $\sim$80 MeV/m. While cryogenic RF cavities have shown improvements to the breakdown limit [7], even larger gains in accelerating electric fields are necessary to enable the next generation of TeV-class machines with reasonable cost and physical footprint. Advanced acceleration methods based on wakefields in a variety of media are capable of generating accelerating gradients up to three orders of magnitude greater than present RF-based accelerators, offering a path to more compact and affordable high-energy physics instruments. For example, the concept of a high-gradient, wakefield-based "afterburner" [8,9], where the terminal energy of a relativistic beam from an existing accelerator facility is multiplied severalfold beyond the design energy of the machine, is an attractive approach for a future e^+e^- linear collider.

Wakefield acceleration techniques use one or more moderate energy *driver* bunches to excite electromagnetic fields, which can accelerate a trailing *witness* bunch by extracting energy from the driver, essentially transforming a high-current, low-voltage system into a relatively lower current, high-voltage system. Plasma wakefield acceleration (PWFA) has demonstrated $>$ GV/m accelerating gradients [10–12] by exciting a nonlinear plasma oscillation, where the plasma electrons are evacuated from the beam channel via the repulsing space charge of the electron bunch driver. This leaves a positively charged ion column, resulting in a linear restoring force on the beam electrons. Such a configuration is able to provide both strong accelerating gradients and linear focusing fields for the body of the driver, as well as for electron witness bunches. However, the nonlinear beam–plasma interaction is not symmetric for positively charged witness beams, e.g., beams of positrons. Reconfiguration of the plasma profile geometry to that of a hollow-core column alleviates some issues related to positively charged beams and has shown experimental progress [13,14], yet stable positron acceleration in a PWFA remains an urgent challenge under study [15,16]. Dielectric wakefield acceleration (DWA), in contrast, relies on wakefields excited by a driver bunch in a solid-state dielectric structure rather than a plasma. High-gradient (GeV/m-class) acceleration of electrons has been demonstrated in dielectric wakefield accelerators [17] but, prior to this work, only electron bunches have been used in DWA. In light of the plasma wakefield accelerator challenges described above, DWA has advantages for use as a positron accelerator because, in the linear limit, DWA is independent of charge-sign and can

accelerate positrons with no fundamental change in the layout of the interaction. Experimentally observed high-field damping effects in electron-driven DWA [18] provide a currently presumed practical limit to the operational gradient; in simple cylindrical SiO_2 DWA geometries, this is near 850 MeV/m. It has not yet been established whether this highly nonlinear process has a charge-sign dependence which may lower this threshold. The exploration of very high fields driven by positron wakes is technically very challenging, as recently illustrated by positron-driven PWFA work, which was accomplished at the same frontier laboratory facility, FACET, as the experiments reported here. As such, the present work concentrates on excitation of gradients, which while well above those of current accelerators are below the onset of effects in the electron-driven case.

We thus report here the first demonstration of high-gradient DWA driven by a positron beam at field levels relevant to the acceleration gradient desired in the range of 500 MeV/m, indeed comparable to that demonstrated previously with plasma-based positron acceleration (inferred 230 MeV/m deceleration gradient in Ref. [13]). We establish that the positron excitation of the modes is functionally equivalent to electron-driven cases at this gradient level. The results we report here should be considered a first exploration of the relevant parameter space for positron acceleration in DWA; further, future investigation of higher field scenarios is discussed in the conclusions. This is an important initial step in understanding relevant effects on relativistic positron beam propagation in a collider-relevant parameter regime, a necessary milestone on the road toward development of an e^+-e^- collider based on DWA technology.

II. EXPERIMENTAL METHODS

The issues related to charge symmetry in the DWA are examined in a set of experiments conducted at the Facility for Advanced Accelerator Experimental Tests (FACET) at SLAC National Accelerator Laboratory [19]. The facility employs high-energy electron and positron bunch modalities enabling a variety of studies. In the positron bunch DWA experiment, accessible properties of the excited wakefields are characterized, and compared with those excited by electron bunches. When establishing the positron bunch parameters, it is important as noted above to operate at accelerating gradients below the threshold for the onset of high-field damping effects in dielectrics [18]. Also, one should employ a suitable dielectric media to avoid potential field emission from the bulk material due to the high fields generated by the positron beam. Finally, demonstrating equal charge-sign response requires employing statistical equivalence tests in data analysis, because the positron and electron data sets were acquired at different times under subtly differing systematic conditions.

At FACET, positron beams are generated by colliding a 20 GeV electron beam onto a tungsten alloy target, creating e^+-e^- pairs. The positrons are then collected, cooled, and transported to the interaction region [20]. For the set of experiments, for both electron and positron drive bunches, the initial energy was 20 GeV with $N_b = 0.7 \times 10^{10}$ particles per bunch, and $\sigma_x = \sigma_y = \sigma_z \approx 40\ \mu$m. The DWA structure consists of silicon dioxide (SiO_2), a nonpolar material, in

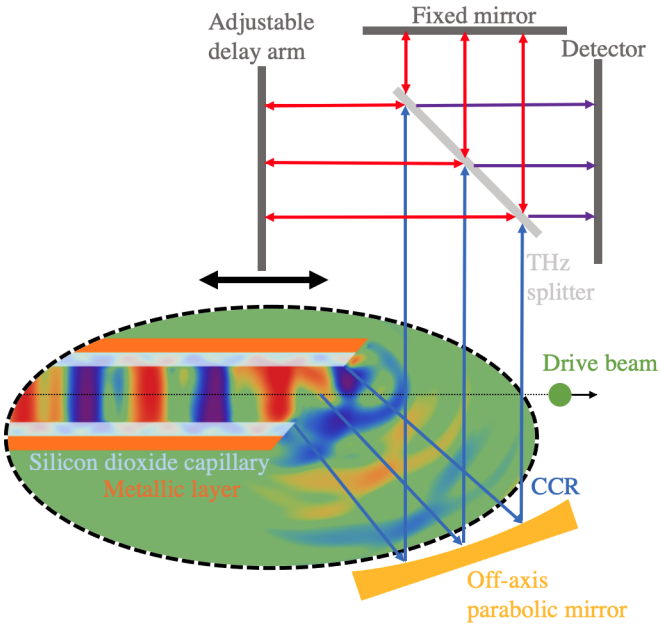

FIG. 1. (Not to scale) Schematic overview of the experiment. The particle beam excites CCR in the dielectric-lined waveguide (shown with E_z fields from numerical simulations) which is quasioptically propagated to a THz interferometer.

a cylindrical geometry. The SiO_2 capillary is coated on the outer wall with a ~10-μm-thick copper layer. The inner and outer radii of the dielectric structures are approximately 200 μm and 300 μm, respectively (i.e., having a 100-μm wall thickness), with an overall length of 3 cm. As the beam transits the dielectric structure, coherent Cerenkov radiation (CCR) is excited within the dielectric [21–24]; for the parameters of this experiment, the CCR is in the terahertz band. The radiation propagates forward and is launched from the end of the tube, which is impedance matched to free space with a Vlasov-type antenna [25]. The CCR is propagated quasioptically using a short-focal-length off-axis parabolic mirror to the main diagnostic, a THz-sensitive interferometer (see Fig. 1 for a schematic overview of the experiment). An autocorrelation-based interferogram is produced on a multishot basis by scanning the delay arm. Pyroelectric detectors, coated for enhanced sensitivity in the THz spectral range, are used in the interferometer. The interferometer signal is processed to calculate the spectral content of the radiation, which aids in revealing the presence of high-field damping [17,18] or additional modes excited by off-axis propagation.

For a dielectric-lined waveguide with cylindrical geometry, the TM-mode (accelerating) frequencies are given by the solutions that satisfy the dispersion relation [26]

$$\frac{I_1(k_1 a)}{I_0(k_1 a)} = \frac{\epsilon_r k_1}{k_2} \frac{J_0(k_2 b)Y_1(k_2 a) - J_1(k_2 a)Y_0(k_2 b)}{J_0(k_2 b)Y_0(k_2 a) - J_0(k_2 a)Y_0(k_2 b)} \quad (1)$$

where k_1 and k_2 are the radial wave numbers in the vacuum and dielectric, respectively; ϵ_r is the dielectric constant (3.8 for SiO_2); a and b are the inner and outer radii of the tube; and I_n, J_n, Y_n are Bessel functions. The solutions to Eq. (1) describe the allowed longitudinal modes in the structure of a given geometry. The convolution of these functions with the temporal

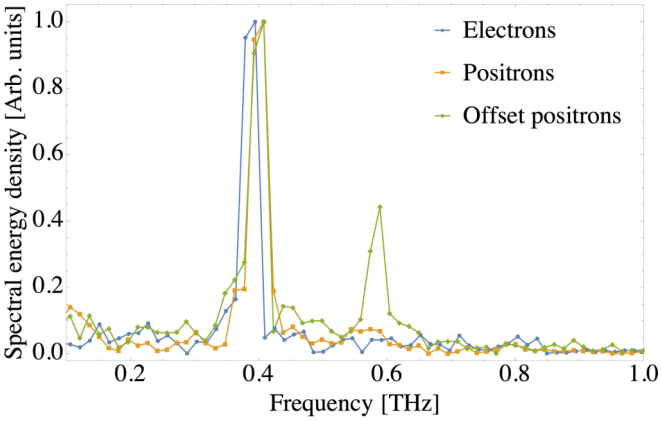

FIG. 2. Average CCR spectra for electrons and positrons on axis, as well as positrons 60 μm off axis. The peak in all cases has been normalized to one.

profile of the driver beam yields the excited wakefields. In this limit, the absorptive effects of the dielectric and the finite conductivity of the metal cladding can be neglected, and as in previous experimental cases with similar parameters [17,22], employing the simple model yields sufficient accuracy [27]. For the scenario described, this expression estimates that the fundamental frequency, TM_{01}, is 393 GHz.

The CCR autocorrelation data were collected by the interferometer in steps of 42 μm, recording several shots per delay. The resulting data set was Fourier transformed to yield the spectra shown in Fig. 2. Fitting the fundamental mode peaks for the electron and positron runs gives estimates for the structures' fundamental modes of 387 and 400 GHz, respectively, in good agreement with the analytic value. Slightly differing cylindrical structures were used for the positron and electron data sets and the frequency discrepancy in measurements is attributable to a spread in tube dimensions consistent with manufacturing tolerances; a 4 μm difference in radius, within the manufacturing tolerance, yields 13 GHz variation in frequency. To permit comparative analysis, the autocorrelation data for the on-axis electron and positron runs were scaled to compensate for the observed frequency difference and then normalized in amplitude and offset to minimize the mean average error with the results shown in Fig. 3.

III. RESULTS AND ANALYSIS

One effect that should be considered is the onset of high-field damping in SiO_2 DWA structures. In previous studies, it was discovered that the damping has a threshold value ($|E_z| \approx 850$ MV/m [18]) for electron drivers. To orient ourselves to the relevant fields achieved in the experiment, the peak longitudinal field in a DWA driven by a Gaussian beam can be estimated by [21]

$$E_z \approx \left| \frac{4N_b r_e m_e c^2}{a q_e \left(\sqrt{\frac{8\pi}{\epsilon_r - 1}} \epsilon_r \sigma_z + a \right)} \right|, \tag{2}$$

where N_b is the number of particles in the drive bunch, r_e is the classical electron radius, m_e is the electron mass, and q_e is the electron charge. For these measurements, this estimate yields 300 MV/m. However, simulations reveal that higher-order modes are being excited, increasing the peak field to 500 MV/m (see Fig. 4). This value is chosen because it is comfortably below the threshold for the onset of high-field damping yet still quite significant for high-gradient acceleration; this gradient is indeed comparable to recent experiments on positron PWFA [13]. The interferograms in Fig. 3 agree with expected results and do not display the characteristic, strong decay signature of induced conductivity-enabled damping. Furthermore, as evident in Fig. 3, the interferograms generated by positrons compared with those generated by electrons do not reveal evidence of charge-dependent effects. The statistical equivalence of the interferogram data is rigorously demonstrated below.

The electron and positron data can be demonstrated to be statistically equivalent but, due to the nature of the data and the fact that different structures were used at different times, direct application of typical statistical analytic approaches, such as paired tests, is not appropriate. Instead, a two one-sided equivalence test is performed on transformed populations. For each delay arm position, multiple shots are recorded (5 for the electron data set, 10 for the positron data set) but these delay arm positions are not the same between data sets. The interferometer reading from each of these shots is denoted as $a_{\{e,p\},k}(z_i)$ where e or p indicates the species as either electrons or positrons, respectively; k is the shot number

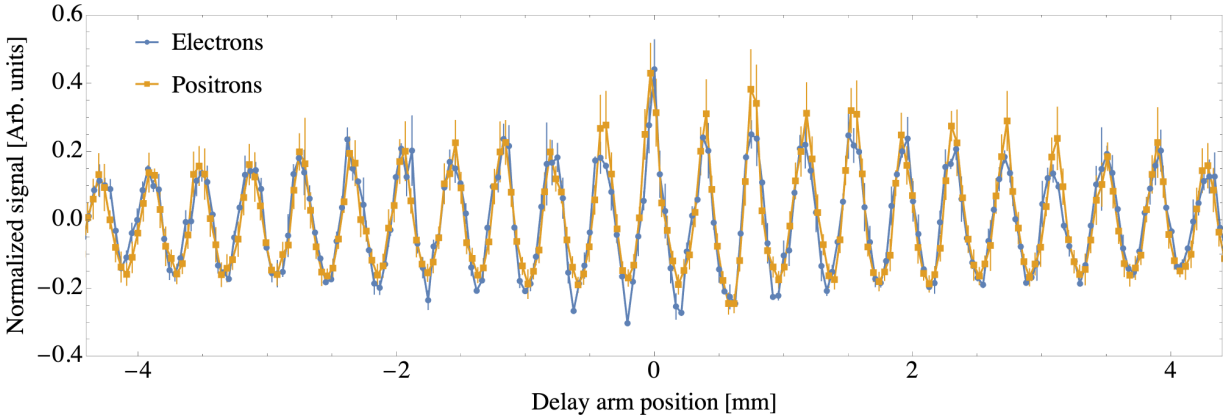

FIG. 3. Frequency scaled and amplitude normalized interferograms for on-axis electrons and positrons, shown with one standard deviation error bars. The connecting lines show the linear interpolations, $m_{\{e,p\}}(z)$, employed by the statistical analysis.

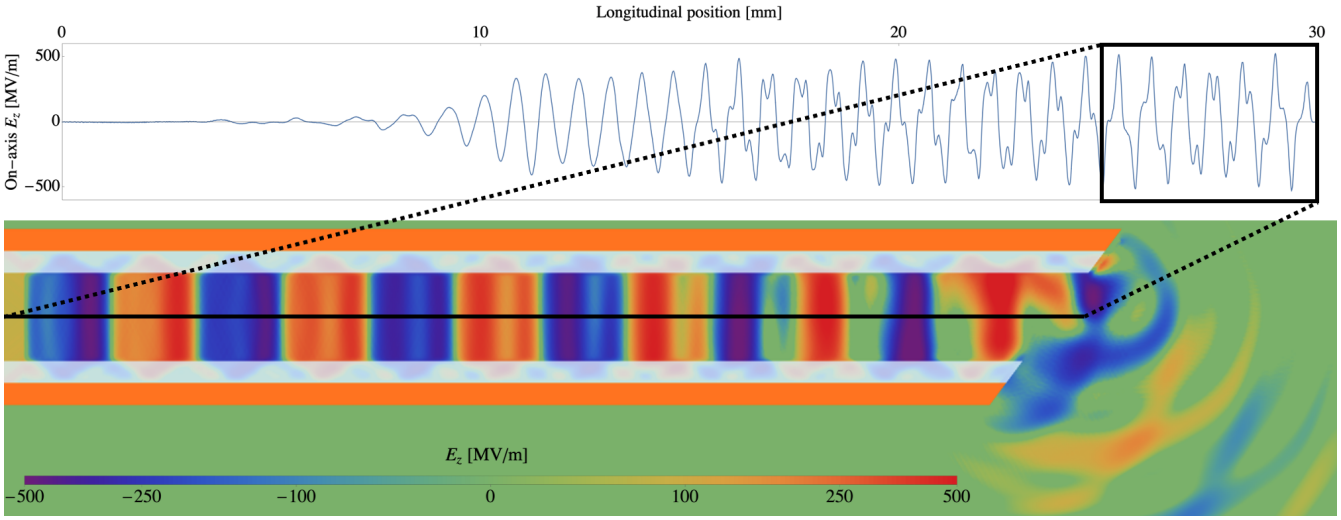

FIG. 4. PIC simulation of on-axis DWA. **Top:** Longitudinal electric field, E_z, measured on axis along the length of the dielectric structure. The excitation of higher modes leads to a higher peak value than predicted by Eq. (2). **Bottom:** Cross-section of the last 5 mm of the dielectric structure showing the E_z fields, illustrating how the CCR excited inside the structure is coupled out into free space for measurement.

at that position; and z_i is the physical location of the delay arm for the ith delay arm position. For each species, at each position, we calculate the median of these values; a linear interpolation of these medians in z yields two continuous functions with respect to delay arm position: $m_{\{e,p\}}(z)$. The mean trend line is defined $m_t(z) \equiv \frac{1}{2}(m_e(z) + m_p(z))$. The trend line is subtracted from each measurement creating two new populations,

$$a'_{\{e,p\},k}(z_i) = a_{\{e,p\},k}(z_i) - m_t(z_i), \tag{3}$$

shown in Fig. 5. By applying a two one-sided test [28,29] to these transformed populations, we can demonstrate the equivalence of the electron and positron responses. To this end, we assert that the smallest effect size of interest (SESOI) is 0.05 (in the units of Fig. 3), approximately equal to the per-position standard deviation for both species. The null hypothesis, H_0, is that of nonequivalence to a meaningful extent, i.e., $|\mu_e - \mu_p| \geqslant$ SESOI, where μ_e and μ_p are the means of the transformed populations a'_e and a'_p, respectively, while the alternative hypothesis, H_A, is that of effective equivalence, $|\mu_e - \mu_p| <$ SESOI. At the 95% confidence level ($p = 0.000$) we may reject the null hypothesis and conclude that the electron and positron responses are functionally equivalent.

This experimental scenario was also simulated using a particle-in-cell (PIC) code, CST [30]. Figure 4 shows the on-axis longitudinal field, E_z, and illustrates that higher-order modes are excited, with peak fields reaching, as noted above, 500 MV/m. The nature of the Vlasov antenna CCR outcoupling is also illustrated with the radiation propagating quasioptically to the interferometer diagnostic. The spectrum of these free-space fields is calculated and shown in Fig. 6; the TM_{01} frequency agrees with the analytic estimate of Eq. (1) and the measured positron and electron spectra.

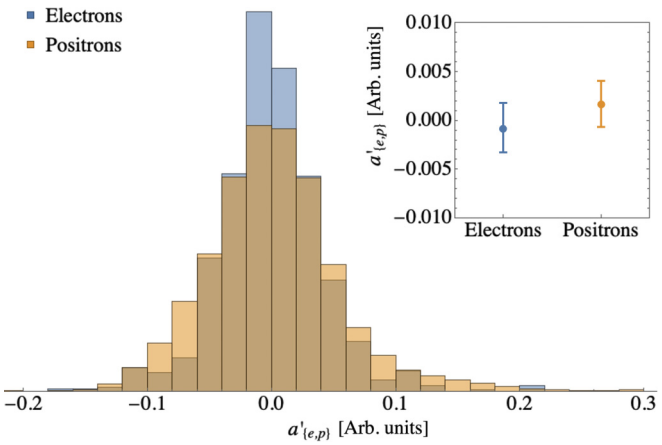

FIG. 5. Histogram showing the data from Fig. 3, transformed according to Eq. (3). The vertical axis is scaled for each population according to the total number of samples. **Inset:** Mean values of these transformed points with 95% confidence interval bars.

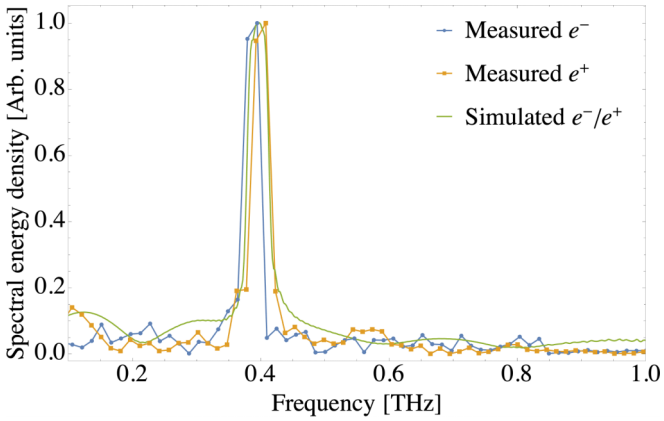

FIG. 6. Average CCR spectra for electrons and positrons on axis, shown with the spectrum of a PIC simulation of this scenario. No charge-sign symmetry-breaking effects were included in the simulation so the results are the same for both electrons and positrons. The peak in all cases has been normalized to one

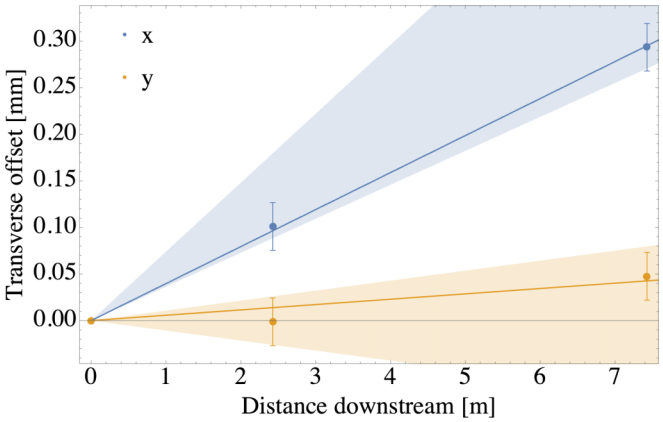

FIG. 7. With the positron beam nominally positioned 60 μm off axis in the x direction, the beam centroids are measured downstream relative to the no-structure positions using BPMs. These positions are shown as points, with 1 standard deviation error bars, and a linear fit. CST simulations were performed for this offset beam, incorporating uncertainty in other experimental parameters, and the simulated centroid positions are shown as colored regions.

In addition to acceleration from longitudinal fields, high-frequency dielectric structures also generate commensurately large transverse fields [31,32]. For the nominal structure dimensions, the HEM_{12} mode is, for linear response, expected to have a frequency of 569 GHz, consistent with the measured value for a positron beam propagated 60 μm off axis (Fig. 2) of 584 GHz. As with the TM modes, this difference is attributed to the manufacturing tolerances of the capillaries. With the structure nominally positioned off the beam axis by 60 μm in the x direction, the position of the beam centroid is measured by two downstream beam position monitors (BPM) after free-space transport. These results, shown in Fig. 7, can be compared with CST simulations of the same scenario, which incorporate uncertainty in experimental parameters, namely, the structure position. During the alignment of on-axis runs, the structure position has feedback in terms of minimizing the beam deflection on the BPMs but for off-axis runs, the position must be dead reckoned, leading to greater uncertainty.

IV. DISCUSSION

These results provide key experimental support for the proposed application of DWA in a future e^+e^- collider operated at high accelerating gradient in a regime relevant to current designs [33], where head-on interactions with witness beams in the 0.8–3.2 nC range are conceptualized to achieve high luminosity. Gradients competitive with reported positron-driven PWFA [13] are inferred without the onset of anomalies associated with known nonlinear effects. The positron-driven wakefields described in this article are analogous to those induced by the positron witness beams in such a collider and our results provide evidence that long-range acceleration may be achieved without disruption by charge-sign-specific, higher-order effects. We demonstrate that positron-driven DWA fields behave in an equivalent fashion to electron-driven DWA fields, as confirmed by the modal analysis, for gradients up to 500 MeV/m and with collider-relevant bunch size and charge in a relatively simple accelerating medium compared with formation of sophisticated plasma configurations for PWFA [13–15].

With these results in hand, a scenario where both electrons and positrons can attain high final energy before interaction, with similar dielectric-lined structures, may be enabled. This approach can reduce the final footprint of the collider accelerators by at least one order of magnitude beyond the current state of the art. The degree of this reduction in size is dependent on demonstrated effects such as high-field damping and as yet unexplored effects. For example, field emission driven by the intense electric field from a positively charged bunch should be considered as a possibility at very high fields. Indeed, continued experimental investigations on positron-driven DWA are planned to explore the possible onset of possible charge-sign-dependent effects. Upcoming experiments at FACET-II [34] aim to excite and characterize such effects by driving higher strength wakefields in smaller structures and exploring different media responses. These effects may include the above-mentioned damping [18] or the emission of electrons from the dielectric surface into the DWA vacuum channel. These dark-current electrons may be pulled from the dielectric by strong, radial fields instead of by ionization of residual gas and may subsequently induce an electron-cloud-like interaction [35]. This mechanism clearly differs when changing the charge-sign of the beam and thus merits investigation. We note that high-field damping and electron-cloud formation may be mitigated by the introduction of advanced dielectric structures [36,37], high band-gap materials [38], or cryogenic cooling. Additionally, field emission effects may be controllable by shaping the electric field or by choice of dielectric material, so the use of advanced diagnostic techniques for precise spectral characterization is critical for high-frequency structures [39].

ACKNOWLEDGMENTS

We thank Dr. Fred J. Hickernell of the Illinois Institute of Technology for valuable discussions on statistical analysis. This work was supported by the Department of Energy High Energy Physics Grant DE-SC0009914.

[1] R. Barate, The ALEPH Collaboration *et al.*, Measurement of the W mass and width in e^+e^- collisions at 189 GeV, Eur. Phys. J. C **17**, 241 (2000).

[2] T. Barklow, K. Fujii, S. Jung, M. E. Peskin, and J. Tian, Model-independent determination of the triple higgs coupling at e^+e^- colliders, Phys. Rev. D **97**, 053004 (2018).

[3] Y. J. Chae and M. Perelstein, Dark matter search at a linear collider: effective operator approach, J. High Energy Phys. 05 (2013) 138.

[4] Z. Liu, L.-T. Wang, and H. Zhang, Exotic decays of the 125 gev higgs boson at future e+e- colliders, Chin. Phys. C **41**, 063102 (2017).

[5] T. Behnke *et al.*, The international linear collider technical design report-volume 1: Executive summary., arXiv:1306.6327.

[6] L. Linssen, A. Miyamoto, M. Stanitzki, and H. Weerts (Eds.), Physics and detectors at clic: Clic conceptual design report (2012), arXiv:1202.5940

[7] A. D. Cahill, J. B. Rosenzweig, V. A. Dolgashev, S. G. Tantawi, and S. Weathersby, High gradient experiments with X-band cryogenic copper accelerating cavities, Phys. Rev. Accel. Beams **21**, 102002 (2018).

[8] S. Lee, T. Katsouleas, P. Muggli, W. Mori, C. Joshi, R. Hemker, E. Dodd, C. Clayton, K. Marsh, B. Blue *et al.*, Energy doubler for a linear collider, Phys. Rev. ST Accel. Beams **5**, 011001 (2002).

[9] M. C. Thompson, H. Badakov, J. B. Rosenzweig, G. Travis, M. Hogan, R. Ischebeck, N. Kirby, R. Siemann, D. Walz, P. Muggli *et al.*, Ultra-high gradient dielectric wakefield accelerator experiments, in *Advanced Accelerator Concepts: 12th Advanced Accelerator Concepts Workshop*, edited by M. Conde and C. Eyberger, AIP Conf. Proc. No. 877 (AIP, New York, 2006), p. 903.

[10] M. Litos, E. Adli, W. An, C. Clarke, C. Clayton, S. Corde, J. Delahaye, R. England, A. Fisher, J. Frederico *et al.*, High-efficiency acceleration of an electron beam in a plasma wakefield accelerator, Nature (London) **515**, 92 (2014).

[11] I. Blumenfeld, C. E. Clayton, F.-J. Decker, M. J. Hogan, C. Huang, R. Ischebeck, R. Iverson, C. Joshi, T. Katsouleas, N. Kirby *et al.*, Energy doubling of 42 gev electrons in a metre-scale plasma wakefield accelerator, Nature (London) **445**, 741 (2007).

[12] A. Deng, O. Karger, T. Heinemann, A. Knetsch, P. Scherkl, G. G. Manahan, A. Beaton, D. Ullmann, G. Wittig, A. F. Habib *et al.*, Generation and acceleration of electron bunches from a plasma photocathode, Nat. Phys. **15**, 1156 (2019).

[13] S. Gessner, E. Adli, J. M. Allen, W. An, C. I. Clarke, C. E. Clayton, S. Corde, J. Delahaye, J. Frederico, S. Z. Green *et al.*, Demonstration of a positron beam-driven hollow channel plasma wakefield accelerator, Nat. Commun. **7**, 11785 (2016).

[14] A. Doche, C. Beekman, S. Corde, J. Allen, C. Clarke, J. Frederico, S. Gessner, S. Green, M. Hogan, B. O'Shea *et al.*, Acceleration of a trailing positron bunch in a plasma wakefield accelerator, Sci. Rep. **7**, 14180 (2017).

[15] T. Silva, L. D. Amorim, M. C. Downer, M. J. Hogan, V. Yakimenko, R. Zgadzaj, and J. Vieira, Stable Positron Acceleration in Thin, Warm, Hollow Plasma Channels, Phys. Rev. Lett. **127**, 104801 (2021).

[16] C. A. Lindstrøm, E. Adli, J. M. Allen, W. An, C. Beekman, C. I. Clarke, C. E. Clayton, S. Corde, A. Doche, J. Frederico, S. J. Gessner, S. Z. Green, M. J. Hogan, C. Joshi, M. Litos, W. Lu, K. A. Marsh, W. B. Mori, B. D. OShea, N. Vafaei-Najafabadi *et al.*, Measurement of Transverse Wakefields Induced by a Misaligned Positron Bunch in a Hollow Channel Plasma Accelerator, Phys. Rev. Lett. **120**, 124802 (2018).

[17] B. O'Shea, G. Andonian, S. K. Barber, K. L. Fitzmorris, S. Hakimi, J. Harrison, P. D. Hoang, M. J. Hogan, B. Naranjo, O. B. Williams *et al.*, Observation of acceleration and deceleration in gigaelectron-volt-per-metre gradient dielectric wakefield accelerators, Nat. Commun. **7**, 12763 (2016).

[18] B. D. O'Shea, G. Andonian, S. K. Barber, C. I. Clarke, P. D. Hoang, M. J. Hogan, B. Naranjo, O. B. Williams, V. Yakimenko, and J. B. Rosenzweig, Conductivity Induced by High-Field Terahertz Waves in Dielectric Material, Phys. Rev. Lett. **123**, 134801 (2019).

[19] M. J. Hogan, T. O. Raubenheimer, A. Seryi, P. Muggli, T. Katsouleas, C. Huang, W. Lu, W. An, K. A. Marsh, W. B. Mori, C. E. Clayton, and C. Joshi, Plasma wakefield acceleration experiments at FACET, New J. Phys. **12**, 055030 (2010).

[20] R. Erickson, SLC Design Handbook, Tech. Rep. (Stanford Linear Accelerator Center, 2004).

[21] M. C. Thompson, H. Badakov, A. M. Cook, J. B. Rosenzweig, R. Tikhoplav, G. Travish, I. Blumenfeld, M. J. Hogan, R. Ischebeck, N. Kirby, R. Siemann, D. Walz, P. Muggli, A. Scott, and R. B. Yoder, Breakdown Limits On Gigavolt-Per-Meter Electron-Beam-Driven Wakefields in Dielectric Structures, Phys. Rev. Lett. **100**, 214801 (2008).

[22] A. M. Cook, R. Tikhoplav, S. Y. Tochitsky, G. Travish, O. B. Williams, and J. B. Rosenzweig, Observation of Narrow-Band Terahertz Coherent Cherenkov Radiation from a Cylindrical Dielectric-Lined Waveguide, Phys. Rev. Lett. **103**, 095003 (2009).

[23] G. Andonian, Electron-beam driven dielectric wakefield accelerator experiments in the terahertz regime, in *Advanced Accelerator Concepts: 15th Advanced Accelerator Concepts Workshop*, edited by R. Zgadzaj, E. Gaul, and M. C. Downer, AIP Conf. Proc. No. 1507 (AIP, New York, 2012), p. 94.

[24] K. Floettmann, F. Lemery, M. Dohlus, M. Marx, V. Tsakanov, and M. Ivanyan, Superradiant cherenkov–wakefield radiation as thz source for fel facilities, J. Synchrotron Radiat. **28**, 18 (2021).

[25] S. N. Vlasov and I. M. Orlova, Optical transformer which transforms the waves in a waveguide having a circular cross section into a highly directional wave beam, Radiophys. Quantum Electron. **17**, 115 (1974).

[26] T.-B. Zhang, T. Marshall, and J. Hirshfield, A cerenkov source of high-power picosecond pulsed microwaves, IEEE Trans. Plasma Sci. **26**, 787 (1998).

[27] M. I. Ivanyan, L. V. Aslyan, K. Floettmann, F. Lemery, and V. M. Tsakanov, Wakefields in conducting waveguides with a lossy dielectric channel, Phys. Rev. Accel. Beams **23**, 041301 (2020).

[28] W. W. Hauck and S. Anderson, A new statistical procedure for testing equivalence in two-group comparative bioavailability trials, J. Pharmacokinet. Biopharm. **12**, 83 (1984).

[29] D. Lakens, A. M. Scheel, and P. M. Isager, Equivalence testing for psychological research: A tutorial, Adv. Meth. Pract. Psychol. **1**, 259 (2018).

[30] CST studio suite – electromagnetic field simulation software, https://www.3ds.com/products-services/simulia/products/cst-studio-suite/.

[31] S. Bettoni, P. Craievich, A. A. Lutman, and M. Pedrozzi, Temporal profile measurements of relativistic electron bunch based on wakefield generation, Phys. Rev. Accel. Beams **19**, 021304 (2016).

[32] B. D. O'Shea, G. Andonian, S. S. Baturin, C. I. Clarke, P. D. Hoang, M. J. Hogan, B. Naranjo, O. B. Williams, V. Yakimenko, and J. B. Rosenzweig, Suppression of Deflecting Forces in Planar-Symmetric Dielectric Wakefield Accelerating Structures with Elliptical Bunches, Phys. Rev. Lett. **124**, 104801 (2020).

[33] V. Shiltsev and F. Zimmermann, Modern and future colliders, Rev. Mod. Phys. **93**, 015006 (2021).

[34] V. Yakimenko, L. Alsberg, E. Bong, G. Bouchard, C. Clarke, C. Emma, S. Green, C. Hast, M. J. Hogan, J. Seabury, N. Lipkowitz, B. O'Shea, D. Storey, G. White, and G. Yocky, FACET-II facility for advanced accelerator experimental tests, Phys. Rev. Accel. Beams **22**, 101301 (2019).

[35] K. Ohmi, F. Zimmermann, and E. Perevedentsev, Wake-field and fast head-tail instability caused by an electron cloud, Phys. Rev. E **65**, 016502 (2001).

[36] G. Andonian, O. Williams, S. Barber, D. Bruhwiler, P. Favier, M. Fedurin, K. Fitzmorris, A. Fukasawa, P. Hoang, K. Kusche, B. Naranjo, B. O'Shea, P. Stoltz, C. Swinson, A. Valloni, and J. B. Rosenzweig, Planar-Dielectric-Wakefield Accelerator Structure Using Bragg-Reflector Boundaries, Phys. Rev. Lett. **113**, 264801 (2014).

[37] P. D. Hoang, G. Andonian, I. Gadjev, B. Naranjo, Y. Sakai, N. Sudar, O. Williams, M. Fedurin, K. Kusche, C. Swinson, P. Zhang, and J. B. Rosenzweig, Experimental Characterization of Electron-Beam-Driven Wakefield Modes in a Dielectric-Woodpile Cartesian Symmetric Structure, Phys. Rev. Lett. **120**, 164801 (2018).

[38] B. Naranjo, A. Valloni, S. Putterman, and J. B. Rosenzweig, Stable Charged-Particle Acceleration and Focusing in a Laser Accelerator Using Spatial Harmonics, Phys. Rev. Lett. **109**, 164803 (2012).

[39] M. Kellermeier, F. Lemery, K. Floettmann, W. Hillert, and R. Assmann, Self-calibration technique for characterization of integrated thz waveguides, Phys. Rev. Accel. Beams **24**, 122001 (2021).